

Design and experimental validation of a restoring force enhanced RF MEMS capacitive switch with stiction-recovery electrodes

Muhua Li^{1,2,3} · Jiahao Zhao^{1,2,3} · Zheng You^{1,2,3,4} · Guanghong Zhao⁵

Received: 24 May 2016 / Accepted: 13 September 2016 / Published online: 8 October 2016
© Springer-Verlag Berlin Heidelberg 2016

Abstract This paper presents an approach for restoring force enhancement to radio frequency (RF) micro-electro-mechanical systems (MEMS) switch with stiction-recovery actuation mechanism. It is based on additional anti-stiction electrodes which are inserted to the coplanar waveguide (CPW) between the signal line and ground planes of a RF MEMS switch. If the movable membrane sticks to the substrate, electrostatic force, as extra restoring force, generated by the bias voltage between the anti-stiction electrodes can promise restoring action. The designed device with the proposed approach is fabricated. The restoring force of the fabricated device had reached 75, 177 and 520 μN by the bias voltages of 0, 10 and 20 V, respectively.

1 Introduction

Since RF MEMS switches were first demonstrated, they have been extensively studied and regarded as a better candidate to replace mechanical relays and semiconductor

switches due to their superior properties such as low insertion loss, high isolation, high linearity, high integration and low power consumption (Rebeiz et al. 2013; Angira and Rangra 2015; Singh and Rangra 2015). RF MEMS switches have varied applications in high performance wireless communication systems (Patil and Kolhare 2013), automated test equipment, phased arrays (Gong et al. 2011) and reconfigurable apertures for defense systems (Jung et al. 2012). The RF MEMS capacitive switch is a promising MEMS device which controls the RF signal through RF power coupling between the signal line and the MEMS bridge. Compared with the contact switch, the capacitive type is more suitable for high frequency application and can survive from the contact degradation mechanism (van Spengen 2012; Pal et al. 2015). However, it still suffers from stiction which is caused by dielectric charging during operation or capillary forces induced by evaporation of the droplet in the gap (Kim et al. 1998) when sacrificial material is being removed. Stiction problem of the movable electrode is the main threat of a capacitive RF MEMS switch (Goldsmith et al. 2001; Mellé et al. 2005; Yuan et al. 2006), which is very difficult to overcome. Stiction happens when the adhesion force exceed the restoring force of the component. So increasing the restoring force is essential.

The easiest way to increase the restoring force is to design a switch with some micro-structure with higher stiffness, but the actuation voltage of the switch will rise higher with the stiffness. For example, RF MEMS switch products of Radant Company have actuation voltages of several tens of volts to obtain high restoring force for preventing stiction (Radant MEMS 2010). However, high actuation voltage has always hindered RF MEMS switches from being widely used (Yanqing Zhu et al. 2014; Lin et al. 2015), so this strategy is not appropriate for designing MEMS switches.

✉ Jiahao Zhao
falxon@mail.tsinghua.edu.cn

¹ Department of Precision Instrument, Tsinghua University, 100084 Beijing, People's Republic of China

² State Key Laboratory of Precision Measurement Technology and Instruments, 100084 Beijing, People's Republic of China

³ Collaborative Innovation Center for Micro/Nano Fabrication, Device and System, 100084 Beijing, People's Republic of China

⁴ Tsinghua-Berkeley Shenzhen Institute, University Town of Shenzhen, 518055 Shenzhen, People's Republic of China

⁵ Beijing Research Institute of Telemetry, Beijing, People's Republic of China

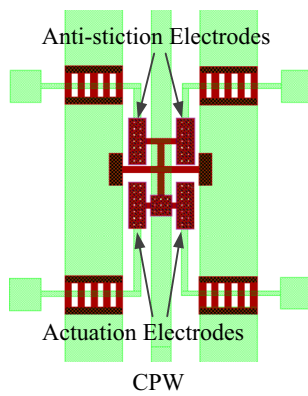


Fig. 1 Top view of the stiction-recovery RF MEMS capacitive switch

Utilizing torsional beams is another way to increase the restoring force. Min-Wu Kim et al. proposed a stiction-recoverable MEMS switch with torsional hinge structures (Kim et al. 2013). With a see-saw configuration and addition anti-stiction electrodes, the restoring force could be increased by biasing the anti-stiction electrodes. However, the detail investigations on restoring force provided by the anti-stiction electrodes have never been reported.

In this paper, an approach to enhance restoring force of the movable electrodes for a RF MEMS capacitive switch is introduced and verified by detail investigations of a fabricated device. The switch in our work is based on a stiction-recovery actuation micro-structure. The major advantage of this design is that the additional stiction-recovery electrodes could provide extra restoring force, besides stiffness of the actuation electrodes. If actuation electrodes adhere to the substrate surface, the switch must be failed without recovery electrodes, but the switch could pull out and work well again by applying DC voltages to the stiction-recovery electrodes. Furthermore, the anti-stiction electrodes are embedded inside the CPW structure between the signal line and ground planes in this design, so the switch structure is compact.

2 Switch design

A schematic diagram of the proposed device is shown in Fig. 1 (Table. 1). The proposed switch is based on a coplanar waveguide, which contains a signal line and two ground planes. Bottom actuation electrodes and stiction-recovery electrodes are located between the signal line and ground planes. There is a torsional beam connecting to anchors that are located on top of ground planes. Top actuation electrodes and stiction-recovery electrodes are located respectively on two ends of the beam. A square plate is connected to upper actuation electrodes in order to offer enough

Table 1 Design parameters of the proposed switch

Serial number	Design parameter	Value	Unit
1	CPW	90–60–90	μm
2	See-saw bridge width	20	μm
3	See-saw bridge length	70	μm
4	Electrode length	140	μm
5	Electrode width	50	μm
6	The air gap	3	μm
7	Membrane thickness	1	μm
8	Dielectric thickness	0.3	μm
9	Dioxide thickness	0.5	μm
10	Thickness of the signal line	1.8	μm

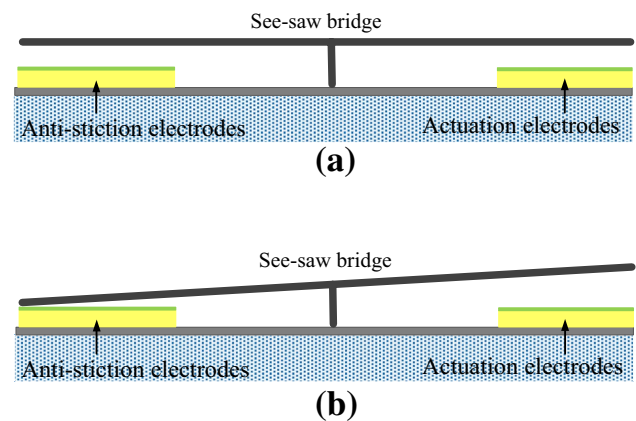


Fig. 2 Cross-sectional view for proposed switch in different working states. **a** ON state **b** stiction-recovery state

capacitance to block the RF signal in the OFF state. Compared with that, stiction-recovery electrodes are connected by a narrow beam to reduce negative effect affecting the RF properties of the switch, and the capacitive overlap area is much smaller than that of actuation electrodes.

The switch has three states: ON state (no DC voltages applied), OFF state (DC voltages applied to the actuation electrodes) and stiction-recovery state (DC voltages applied to the anti-stiction electrodes). When no voltages are applied to the electrode, the switch stays horizontally positioned. The switch is electrostatically actuated by applying a DC voltage to bottom actuation electrodes. After the actuation voltage is applied to bottom actuation electrodes, the switch is actuated and tilted to the actuated side. As long as the switch works normally, anti-stiction electrodes are not used. When the switch membrane sticks to the substrate and cannot return to the original position by its own elastic restoring force, voltages applied to bottom anti-stiction electrodes will pull the top anti-stiction electrodes down, which will produce an upward force to the membrane through the seesaw-like structure.

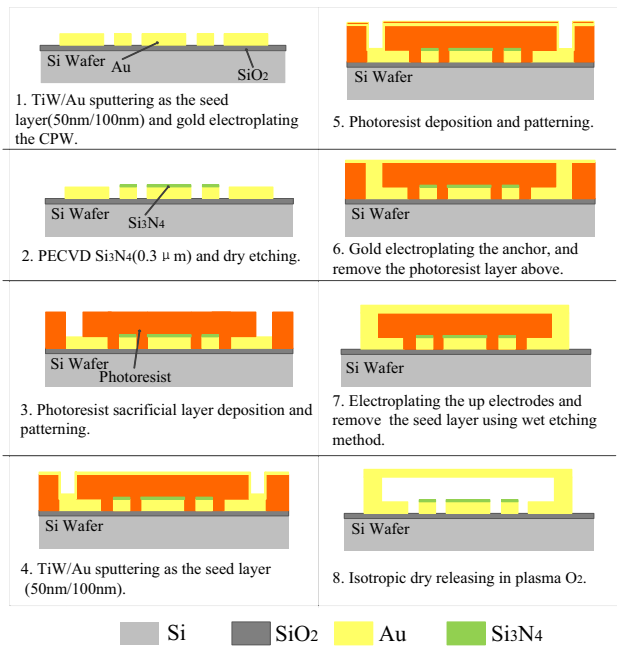


Fig. 3 Main steps of RF MEMS capacitive switch fabrication process flow

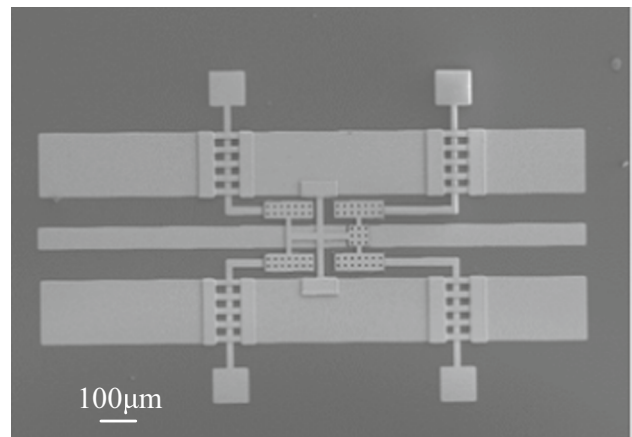
Cantilever connecting the anti-stiction electrodes is the same as the cantilever connecting the actuation electrodes, which means the anti-stiction voltage is the same as the actuation voltage according to the lever principle (Fig. 2).

3 Fabrication process flow

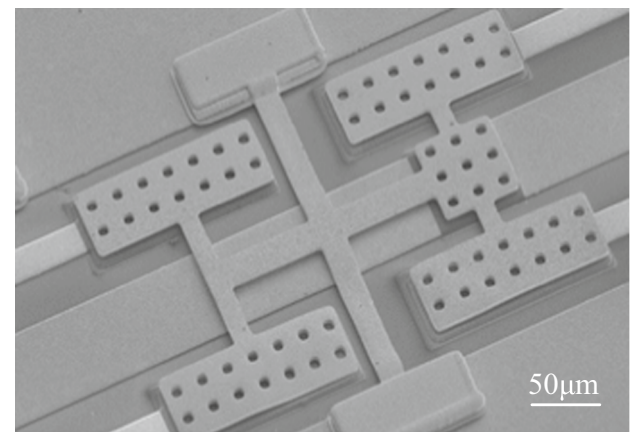
The designed switch was fabricated on high resistivity silicon substrate with a surface-micromachined approach. A five-mask fabrication process was utilized. The main technological steps for the fabrication process are shown in Fig. 3.

Gold is used as the material of CPW and switch structures for its excellent electrical conductivity. The switch is placed on a high-impedance silicon substrate which has a thin layer of silicon dioxide (SiO_2) on it for the purpose of isolation. Silicon nitride (Si_3N_4) is used as the dielectric material.

The first step is creating a thin ($0.5 \mu\text{m}$) thermal silicon oxide to passivate and isolate the substrate surface. Then, a multilayer of TiW/Au ($50/100 \text{ nm}$) is sputtered as the adhesion/seed layer, and the bottom electrodes of the switch is formed by gold-electroplating deposition. The seed layer is removed by inductively coupled plasma (ICP) etching. The process continued with a $0.3 \mu\text{m}$ plasma-enhanced chemical vapor deposited Si_3N_4 ($\epsilon_{\text{Si}_3\text{N}_4} = 7.5$) utilized as the dielectric layer. Si_3N_4 is patterned by Ion Beam Etching (IBE).



(a)



(b)

Fig. 4 Scanning electron microscope (SEM) images. **a** A general view of the RF MEMS switch. **b** Zoom on the membrane

Next, a $3 \mu\text{m}$ photoresist sacrificial layer is deposited and patterned. A multilayer of TiW/Au ($50/100 \text{ nm}$) is sputtered as the adhesion/seed layer. A thin layer of photoresist is deposited and patterned to cover the suspended bridge, without which the bridge will be electroplated together with the anchor in the gold-electroplating process. After the anchor is electroplated, the photoresist mold is removed. Another photoresist layer is deposited and patterned as the electroplating mold of the membrane. Topology of the bridge and release holes are defined by the mold. These holes are used for both releasing the switch structure and improving the switching speed. After the gold-electroplating process, the metal membrane is created. The metal seed layer is removed by wet etching to avoid high temperature created by dry etching, which will affect the sacrificial layer. The final step is removing the photoresist sacrificial by isotropic O_2 plasma dry etching, and the structure is released. SEM images of the fabricated device is shown in Fig. 4.

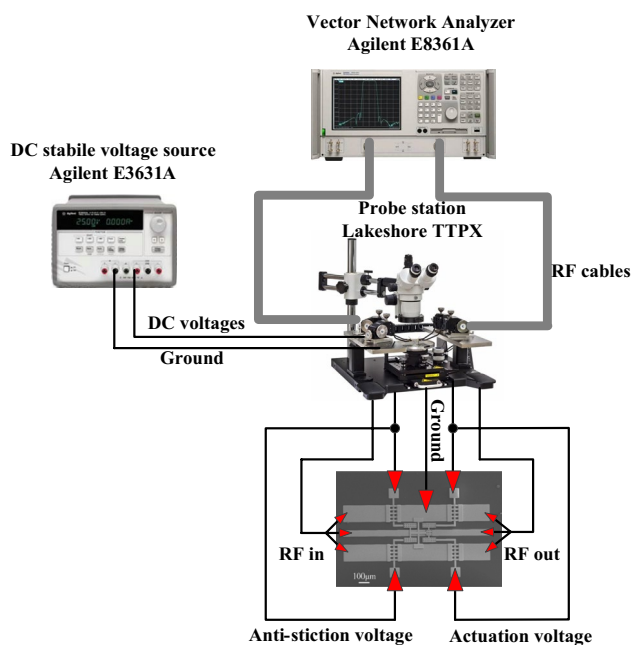


Fig. 5 Measurement setup of RF properties

4 RF performance

The fabricated device discussed in the previous sections is measured under ambient environmental conditions. Electrical properties of the switch is tested using an Agilent Vector Network Analyzer E8361A and a Lakeshore probe station which is equipped with DC probes and ground-signal-ground RF probes. Figure 5 shows the measurement setup.

The switch is electrostatically actuated by applying a DC voltage to the bottom actuation electrodes, and the membrane will bend down. Besides, applying a DC voltage to the bottom stiction-recovery electrodes will pull the top electrodes down, which creates an upward pulling force to the actuation electrode through the seesaw-like structure. Five devices are tested and an average pull-in voltage of 18 V is found.

The insertion loss and isolation of the switch are shown in Fig. 6.

The insertion loss was measured when no voltages were applied to the electrodes, and the isolation was measured when the DC voltages were applied to the bottom actuation electrodes. The proposed switch provides good RF performances with an isolation of -29 dB and an insertion loss of -0.92 dB at 35 GHz.

5 Restoring force measurements

FT-RS 1000 Micro-robotic System is used to measure the restoring force enhancing effects of the anti-stiction

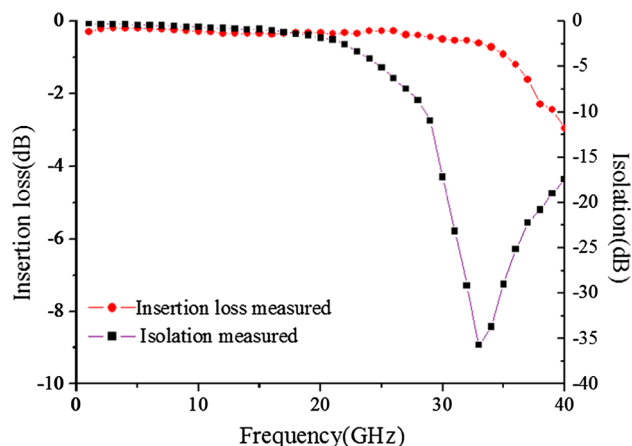


Fig. 6 Measured insertion loss and isolation of the proposed switch

electrodes. The micro-robotic system contains a movable platform and a sensor which is put on a tip of a probe. The probe is connected to the platform through an angle-adjustable arm. The sensor can record both the moving distance and the force when it goes toward a certain direction, so the whole system is always used to measure the stiffness of a MEMS device. The experimental validation of the proposed is realized by three steps. The first step is measuring the stiffness of the substrate and the measurement results contains the contribution of the arm which connects the sensor and the movement platform. The second step is measuring the force-distance relationship of the center plate membrane of the upper actuation electrodes when no voltages are applied to both the actuation electrodes and the anti-stiction electrodes. The third step is measuring the force-distance relationship of the membrane when different voltages are applied to anti-stiction electrodes. If the force rises when anti-stiction voltages are applied, the usefulness of the anti-stiction electrodes is proved. As the substrate and the arm will contribute to the measurement results in step 2 and step 3, its influence is eliminated through data processing after the experiment.

Figure 7 shows the measurement results of the sensor. Before the sensor gets close to the membrane, no force is detected. When the sensor goes near the membrane, the sensor detected a downward force because of the potential difference of the membrane and the sensor. After the sensor contacts the plate, the switch's restoring force is measured. Then sensor will gradually push the membrane to the substrate and record the relationship between the force and the distance. As soon as the membrane touches the substrate, the sensed force increases much faster because the stiffness of the substrate is much bigger than the switch's. The measurement results show that when anti-stiction voltages are applied to the electrodes, the other side of the lever will goes up, and bigger restoring forces are achieved.

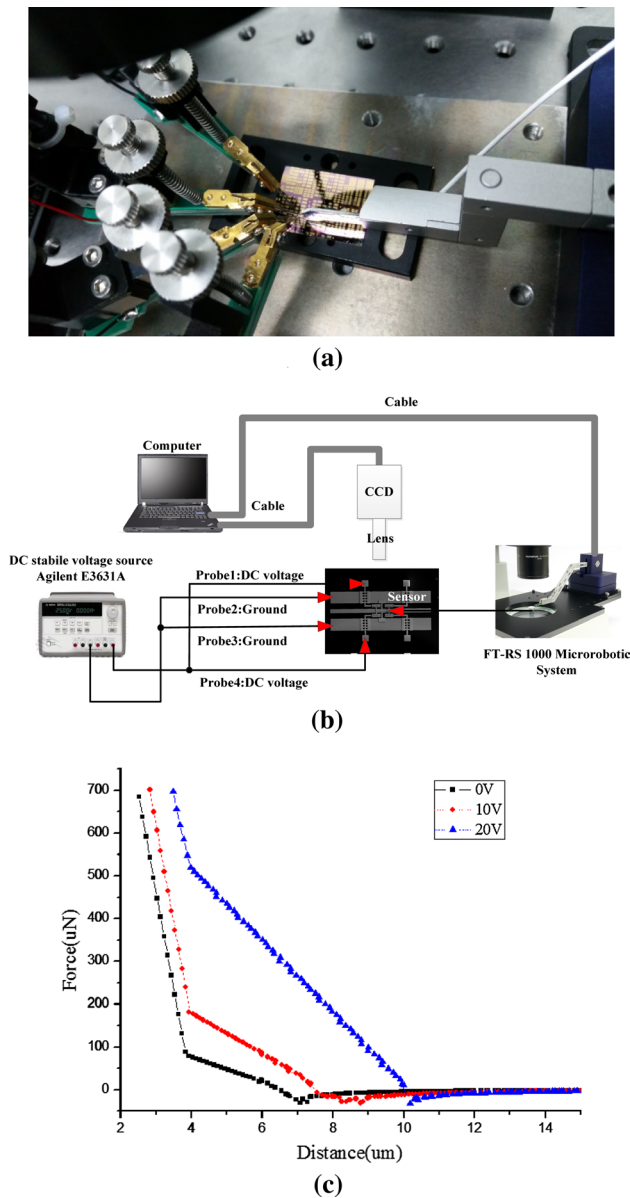


Fig. 7 Measurement setup and results. **a** DC probes and the force sensor. **b** Measurement setup. **c** Force-distance relationship under different anti-stiction voltages

The air gap of the switch is 3 μm , so when no DC voltages are applied, the sensor will go for a distance of 3 μm until the membrane contacts the substrate. However, when DC voltages are applied, the top anti-stiction electrodes will bend down and the actuation side will go up, which causes the sensor to contact the membrane earlier. Forces needed to push the membrane down to the substrate is 75, 177 and 520 μN under voltages of 0, 10 and 20 V. Restoring forces are significantly improved by the anti-stiction voltages, which proves that the proposed switch are easier to recover from stiction problems compared with conventional switches.

6 Conclusion

Stiction failures affect the reliability and working life of RF MEMS switches. In this paper, an approach to enhance restoring force of RF MEMS capacitive switches is presented. The stiction problem can be relieved by anti-stiction actuation mechanisms. The proposed device is designed, fabricated and tested. Additional anti-stiction electrodes and torsional beams are utilized in the switch structure. The fabricated switch's actuation voltage is as low as 18 V. An insertion loss of -0.92 dB and an isolation of -29 dB were obtained at a Ka-band frequency of 35 GHz. Experiment results prove that its restoring force is significantly improved by biasing the anti-stiction electrodes. Compared with the value when no anti-stiction voltage is applied, the restoring force is increased more than one time and six times under 10 and 20 V, respectively.

References

Angira M, Rangra K (2015) A low insertion loss, multi-band, fixed central capacitor based RF-MEMS switch. *Microsyst Technol* 21:2259

Goldsmith C, Ehmke J, Malczewski A, Pillans B, Eshelman S, Yao Z, Brank J, Eberly M (2001) Lifetime characterization of capacitive RF MEMS switches. In: Sigmon B (ed) *IEEE MTT-S International Microwave Symposium Digest*, p 227–230

Gong S, Shen H, Barker NS (2011) A 60-GHz 2-bit switched-line phase shifter using SP4T RF-MEMS switches. *IEEE T Microw Theory* 59:894–900

Jung TJ, Hyeon I, Baek C, Lim S (2012) Circular/linear polarization reconfigurable antenna on simplified RF-MEMS packaging platform in K-band. *IEEE T Antenn Propag* 60:5039–5045

Kim CJ, Kim JY, Sridharan B (1998) Comparative evaluation of drying techniques for surface micromachining. *Sens Actuators A (Physical)* 64:17–26

Kim M-W, Song Y, Yang H, Yoon J (2013) An ultra-low voltage mems switch using stiction-recovery actuation. *J Micromech Microeng* 23:45022–45027

Lin C, Hsu C, Dai C (2015) Fabrication of a micromachined capacitive switch using the CMOS-MEMS technology. *Micromachines* 6:1645

Mellé S, de Conto D, Dubuc D, Grenier K, Vendier O, Muraro J, Cazaux J, Plana R (2005) Reliability modeling of capacitive RF MEMS. *IEEE T Microw Theory* 53:3482–3488

Pal J, Zhu Y, Lu J, Khan F, Dao D (2015) A novel three-state contactless RF micromachined switch for wireless applications. *IEEE Electron Device Lett* 36:1363

Patil GD, Kolhare NR (2013) A review paper on RF MEMS switch for wireless communication. *Int J Eng Trends Technol* 4:195–198

Rebeiz GM, Patel CD, Han SK, Ko C, Ho KMJ (2013) The Search for a Reliable MEMS Switch? *IEEE Microwave Mag* 14:57–67

Singh T, Rangra K (2015) Compact low-loss high-performance single-pole six-throw RF MEMS switch design and modeling for DC to 6 GHz. *Microsyst Technol* 21:2387

van Spengen WM (2012) Capacitive RF MEMS switch dielectric charging and reliability: a critical review with recommendations. *J Micromech Microeng* 22:074001

- SPST RF-MEMS switch dc to 12 GHz RMWS101 Radant MEMS data-sheet. http://www.radantmems.com/radantmems.data/Library/Radant-Datasheet101_1.4.pdf. Accessed 6 Oct 2016
- Yuan X, Peng Z, Hwang JCM, Forehand D, Goldsmith CL (2006) Acceleration of dielectric charging in RF MEMS capacitive switches. *IEEE Trans Device Mater Reliab* 6:556–563
- Zhu Y, Han L, Qin M, Huang Q (2014) Novel DC-40 GHz MEMS series-shunt switch for high isolation and high power applications. *Sens Actuator A* 214:101–110